LAWRENCE
LIVERMORE
NATIONAL
LABORATORY

LLNL-JRNL-764246

High water recovery and improved thermodynamic efficiency for capacitive deionization using variable flowrate operation

A. Ramachandran, D. I. Oyarzun, S. A. Hawks , M. Stadermann, J. G. Santiago

December 17, 2018

Water Research

Disclaimer

High water recovery and improved thermodynamic efficiency for capacitive deionization using variable flowrate operation

Ashwin Ramachandran,[a] Diego I. Oyarzun,[b] Steven A. Hawks,[c] Michael Stadermann,[c] Juan G. Santiago [b,*]

[a] Department of Aeronautics & Astronautics, Stanford University, Stanford, California 94305, United States

[b] Department of Mechanical Engineering, Stanford University, Stanford, California 94305, United States

[c] Lawrence Livermore National Laboratory, 7000 East Avenue, Livermore, CA, 94550, United States

* To whom correspondence should be addressed. E-mail: juan.santiago@stanford.edu

Abstract

Water recovery is a measure of the amount of treated water produced relative to the total amount of water processed through the system, and is an important performance metric for any desalination method. Conventional operating methods for desalination using capacitive deionization (CDI) have so far limited water recovery to be about 50%. To improve water recovery for CDI, we here introduce a new operating scheme based on a variable (in time) flow rate wherein a low flow rate during discharge is used to produce a brine volume which is significantly less than the volume of diluent produced. We demonstrate experimentally and study systematically this novel variable flowrate operating scheme in the framework of both constant current and constant voltage charge-discharge modes. We show that the variable flowrate operation can increase water recovery for

CDI to very high values of ~90% and can improve thermodynamic efficiency by about 2- to 3-fold compared to conventional constant flowrate operation. Importantly, this is achieved with minimal performance reductions in salt removal, energy consumption, and volume throughput. Our work highlights that water recovery can be readily improved for CDI at very minimal additional cost using simple flow control schemes.

Keywords: capacitive deionization; high water recovery; improved thermodynamic efficiency; water desalination; variable flowrate operation.

1. Introduction

Capacitive deionization (CDI) is a burgeoning water desalination technology aimed at energy efficient treatment of brackish water (Anderson et al., 2010; Oren, 2008; Porada et al., 2013). In CDI, feedwater is flowed between (and sometimes through) a pair of porous electrodes, and on application of an external electric current, the ions in solution are electrostatically trapped onto (or regenerated from) the electrodes. CDI operation under dynamic steady state involves cyclic electrical charging and discharging which results in periodic salt removal (freshwater) and regeneration (brine) phases, respectively.

Metrics to evaluate CDI performance include desalination depth (i.e. concentration reduction), volumetric energy consumption, productivity, and water recovery (Hawks et al., 2018b). CDI performance metrics can be significantly affected by the operating method. Operationally, a CDI cell can be dynamically controlled by varying input current/voltage waveforms and varying flowrate of the feed solution. Most of the previous research around development and assessment of operational strategies for CDI has centered around time-varying current/voltage waveforms under constant flowrate conditions (Choi, 2015; García-Quismondo et al., 2016, 2013; Jande and

Kim, 2013; Kang et al., 2014; Qu et al., 2016; Ramachandran et al., 2018a; Zhao et al., 2012). Very little attention has been given to the study of the effects of time-dependent flowrate operations on CDI performance. Recent work (Hawks et al., 2018a; Shang et al., 2017) was aimed at the study of fluid pulsation-type operations wherein short periods of high flow rates (relative to a nominal value) were introduced during a CDI cycle to improve the cycle charge efficiency. However, these studies were limited to cases where the volume of diluent produced was approximately equal to the volume of brine produced. To our knowledge, our is the first quantitative study of variable flow rate operation where low flowrate during discharge is used to achieve brine volumes which are significantly lower than diluent water volume. Further, we present the first systematic study of the effect of variable flow rate schemes on performance metrics around energy and throughput.

Constant flowrate CDI studies have thus so far been limited to a freshwater recovery of about ~50% per desalination cycle. That is, operation such that only half of the processed feedwater is converted to freshwater. Further, improvements in freshwater recovery for CDI can lower the amount of wastewater generated, increase energy efficiency, and lower overall costs of desalination. Hawks et al., 2018b recently discussed a method of defining a variable “threshold” concentration during a CDI cycle to separate desalinated and brine water to increase water recovery. However, the improved water recovery was achieved at the expense of significantly decreased salt removal performance. Interestingly, Dlugolecki et al., 2016 reported water recovery values of 85% achieved using membrane CDI (MCDI); however, systematic details of the electrical and flow rate schemes (and their coordination) are not provided and there was no published analysis of performance trade-offs involved in increasing water recovery.

In this work, we first present a simple control scheme with time-varying flowrates for CDI which produces significantly lower brine volumes compared to diluent water volumes. The operation involves flowing at a nominal flowrate during electrical charging, followed by a decrease in flowrate during the discharge phase (Figure 1). We studied such a scheme under both constant current and constant voltage charge-discharge modes. Our results demonstrate an increased value for water recovery to a maximum of about 90% compared to the more common ~50% typically achieved with conventional constant flowrate operation. Importantly, we show that this high water recovery can be achieved with only negligible tradeoffs with key metrics for energy consumption, salt removal, and throughput. For the first time, we demonstrate that such high freshwater recovery values can be achieved by conventional CDI in a single-pass, continuous flow desalination cycle. Further, we show that the variable flowrate operation introduced here can also increase the thermodynamic efficiency of the desalination process by a factor ~2 to 3-fold compared to the conventional constant flow operation, demonstrating a more efficient separation (desalination) process. Here, the improvement in thermodynamic efficiency is primarily due to an increase in the Gibbs free energy of the separation process for nearly the same energy consumption. We believe that the variable flowrate operation introduced in this work can be easily implemented in all existing CDI systems, resulting in improved water recovery and overall performance. These results should motivate further research into optimized time-varying flowrate control schemes in concert with electrical control schemes for more generalized optimization of CDI systems.

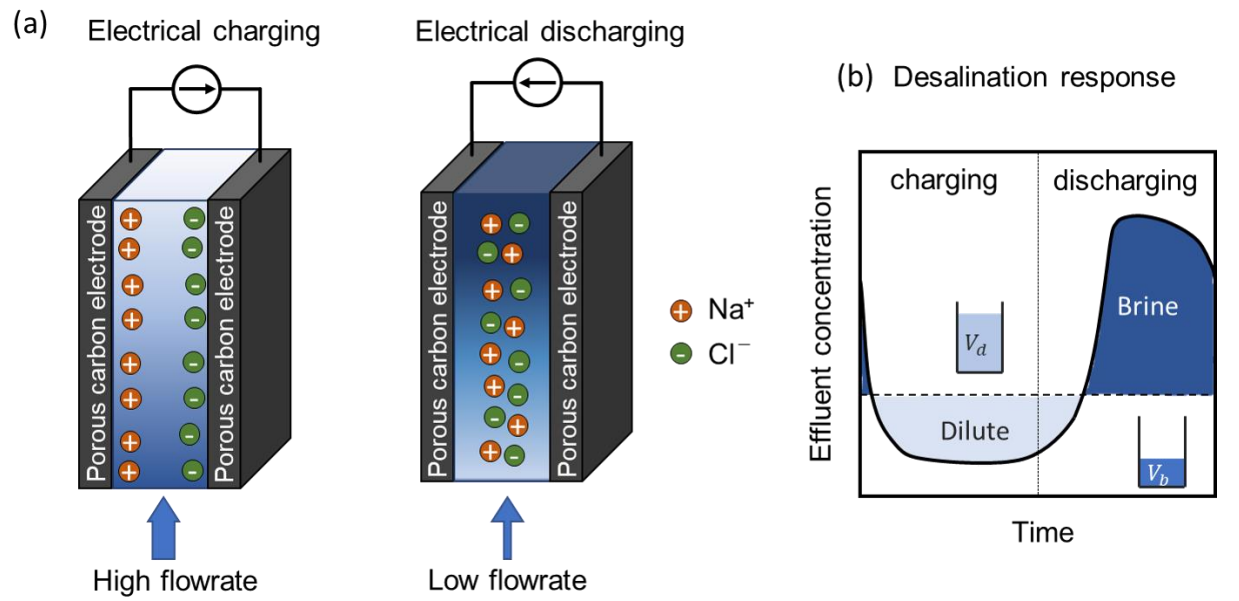

Figure 1. Schematic of (a) flowrate control scheme associated with CDI operation for high water recovery and efficient separation, and (b) typical effluent concentration response versus time for the operation in (a). In (b), the horizontal dashed line indicates feedwater concentration, and V_d and V_b respectively denote the volumes of fresh (dilute) and brine water produced per CDI cycle. During electrical charging, a nominal value of flowrate is used (determined by the desired productivity and average concentration reduction in the freshwater produced). For the discharge (regeneration) phase, a low flowrate (compared to nominal) is used, which results in a low volume of concentrated brine as wastewater.

2. Materials and Methods

2.1 CDI cell fabrication

We assembled a traditional flow-between CDI (fbCDI) cell (no membranes) using a radial-flow architecture as described previously (Biesheuvel and van der Wal, 2010; Hemmatifar et al., 2016; Ramachandran et al., 2018b). Briefly, five pairs of activated carbon electrodes (Materials & Methods, PACMM 203, Irvine, CA) with 5.2 cm diameter, 300 µm thickness, and total dry mass

of 2.7 g were stacked between 4.8 cm diameter, 130 μm thick titanium sheets which acted as current collectors. We used two 180 μm thick non-conductive polypropylene circular meshes (McMaster-Carr, Los Angeles, CA) between each electrode pair as spacers. The spacers had a slightly larger (~5 mm) diameter than the electrodes to prevent electrical short circuits. This assembly was housed inside an acrylic clamshell structure and sealed with O-ring gaskets and fasteners.

We estimate an effective spacer volume of 2.1 ml with a porosity of 55%, and a downstream header volume of 1 ml. The resistance and capacitance of our entire cell were characterized using galvanostatic charging and discharging (see Figures 5 and S3). We estimated an effective capacitance of ~37 F and an effective series resistance of ~1.5 Ohms for 20 mM NaCl.

2.2 Experimental setup

The experimental setup consisted of the CDI cell, a 3 L reservoir filled with 20 mM sodium chloride (NaCl) solution which was circulated in a closed loop, a peristaltic pump (Watson Marlow 120U/DV, Falmouth, Cornwall, UK), a flow-through conductivity sensor (eDAQ, Denistone East, Australia) close to the cell outlet, and a sourcemeter (Keithley 2400, Cleveland, OH). The time-varying current/voltage and flowrate to the cell were controlled using an in-house Python code on a PC which interfaced with the sourcemeter and peristaltic pump. Conductivity measurements were converted to salt concentration using a standard calibration curve. We analyzed the data under dynamic steady state operation conditions (corresponding to the fifth cycle).

2.3 Performance metrics and efficiency measures

We here define four performance metrics and two measures of efficiency for a CDI cell (Hawks et al., 2018b). We will use these to explore system performance and efficiency of desalination for the variable flowrate operation.

First, the productivity *P* is defined as the freshwater production rate per unit cross-sectional area of the electrode, given by

$$P\ [\mathrm{L/h/m^2}] = \frac{V_d}{A t_{cycle}} \tag{1}$$

where V_d is the volume of dilute solution (in L) produced per cycle, t_{cycle} is the total cycle duration (in h), and *A* is the total electrode cross-section area (in m^2). In Equation (1), the "desalination" phase is determined by the total duration in a cycle when the effluent concentration c is less than the feed c_0. The volume of feed solution processed during the desalination phase comprises the dilute volume V_d. The remainder volume V_b processed during the cycle when $c > c_0$ results in concentrated "brine" solution at the effluent.

The second performance metric we use here is *water recovery* (WR) defined as the ratio of dilute water produced to the total feedwater processed per cycle, given by

$$Water\ recovery\ (\%) = \frac{V_d}{V_d + V_b}. \tag{2}$$

Third, to estimate the energy cost, we use *volumetric energy consumption* E_v defined as the net energy spent during a CDI cycle per unit volume of dilute (fresh) water produced, given by

$$E_v[\mathrm{kWh/m^3}] = \frac{\oint_{t_{cycle}} VI\ dt}{3.6E6 \times V_d}, \tag{3}$$

where the integration of instantaneous power supplied to the CDI cell (voltage V times current I) is performed for a complete charge-discharge cycle and V_d has units of m^3.

Fourth, we evaluate the salt removal performance as Δc_d, defined as the *average reduction in the salt concentration* in the desalinated volume compared to the feed solution which is given by

$$\Delta c_d[\mathrm{mM}] = \frac{\int_{t|(c_0-c)>0} Q|c_0 - c|\, dt}{V_d}, \tag{4}$$

where Q is the time-varying flowrate. Likewise, we also report the average increase in concentration of the waste (brine) water Δc_b relative to the feed solution given by

$$\Delta c_b[\mathrm{mM}] = \frac{\int_{t|(c_0-c)<0} Q|c_0 - c|\, dt}{V_b}. \tag{5}$$

We next define two measures of efficiency of the desalination process; namely, the cycle averaged charge efficiency and thermodynamic efficiency.

The cycle charge efficiency Λ is the ratio of moles of removed salt (calculated using the effluent concentration data) to the moles of electronic charge supplied to the electrodes during charging (calculated using the electrical current data), given by

$$\Lambda\,(\%) = F\frac{\int_{t|(c_0-c)>0} Q|c_0 - c|\, dt}{\int_{t|I>0} I\, dt}, \tag{6}$$

where F is the Faraday's constant.

The thermodynamic efficiency η_{th} is defined as the ratio of the Gibbs free energy ΔG_{sep} of the desalination/separation process to the actual volumetric energy consumption calculated from experimental data (using Equation (3)), and is given by

$$\eta_{th}(\%) = \frac{\Delta G_{sep}}{E_v}. \tag{7}$$

In Equation (7), we use

$$\Delta G_{sep} = 2RT\left[c_d \ln c_d + \left(\frac{1}{WR} - 1\right) c_b \ln c_b - \frac{c_0}{WR} \ln c_0\right] \quad (8)$$

where c_d $(= c_0 - \Delta c_d)$ and c_b $(= c_0 + \Delta c_b)$ are respectively the concentrations of the dilute and brine solutions, R is the universal gas constant, and T is the absolute temperature (in K). Refer to (Biesheuvel, 2009; Hemmatifar et al., 2018; Wang et al., 2018) for more details on the derivation and discussion about thermodynamic efficiency for CDI.

3. Results and Discussion

We systematically study and quantify the effect of variable flowrate operation on the desalination performance metrics and efficiencies for conventional constant current (CC) and constant voltage (CV) electrical charge-discharge modes. The variable flowrate operation studied here involves electrical charging at a constant nominal flowrate followed by electrical discharge at a constant but lower value of flowrate.

3.1 Constant voltage electrical charging-discharging with variable flowrate

We performed a series of constant voltage (CV) charge-discharge experiments with a fixed nominal flowrate value of 6 ml/min during charging, and varying discharge flowrate Q_{dc} values of 6, 4.8, 3.6, 2.4, 1.2, 0.6, and 0 ml/min. For a nominal flowrate of 6 ml/min, we estimate a resonant time scale (Ramachandran et al., 2018a) of ~260 seconds. We here studied the variable flowrate operation under two different voltage windows of 0.2-1.0 V and 0.6-1.0 V with 300 s of charging and 300 s of discharging, to ensure "near-resonant" operation (Ramachandran et al., 2018a).

3.1.1 Current and effluent concentration response

Figures 2a and 2b respectively show the current and effluent concentration responses for CV operation between 0.6 -1.0 V for a flowrate of 6 ml/min during charging, and flowrates of 6, 2.4,

and 0.6 ml/min during discharging. The insets in Figures 2a and 2b show plots of the input voltage and flowrate waveforms, respectively. See Figure S1 for results of additional experiments for Q_{dc} values of 4.8, 3.6 and 0 ml/min with a voltage window of 0.6 -1.0 V, and for current and effluent concentration profiles for 0.2 -1.0 V voltage window operation with the same values of Q_{dc}.

The current data of Figure 2a shows that the electrical responses of the cell to significant changes in discharge flowrate are nearly identical. Consequently, the net electrical energy consumption (in Joules) and electrical charge transferred (in Coulombs) per cycle are nearly equal to each other (less than 5% variation) across a wide range of Q_{dc} values between 0 to 6 ml/min (see Figure S2).

On the other hand, Figure 2b shows the profound effects of Q_{dc} on effluent concentration profiles. Effluent concentration during electrical discharge (regeneration phase) increases strongly with decreasing Q_{dc}. The charging phase effluent concentration profiles show only a very weak dependence to changes in discharge-phase flow rate. Further, the peak value of discharge-phase brine concentration also occurs at later times during discharge as Q_{dc} decreases. Lower Q_{dc} also accordingly produces significantly lesser volume of brine during the discharge phase, resulting in a low volume of concentrated brine as wastewater (c.f. inset of Figure 3a).

The start and end of the electrical charge and discharge phases are determined by the times that the forcing voltage switches to maximum and minimum values, respectively. Figure 2b also shows that lowering Q_{dc} influences the relative time delays between the forcing voltages and the output (response) of effluent concentration. Note in Figure 2b the two times at which the effluent concentration crosses the value of the inlet feedwater concentration (denoted as a grey horizontal dotted line). Lower Q_{dc} values and the higher associated values of effluent brine concentration together result in time delays for both of these crossovers, particularly for the crossover which occurs in discharge. This behavior implies that the relative valving between treated and brine

collection downstream should occur at later times for lower Q_{dc}. Lastly, note that, despite these time delays, there is approximate overlap in the times at which effluent concentration is minimum and overlap among the effluent concentration during much of charging phase. In the next subsection, we will present a quantification of the volume of fresh (dilute) and waste (brine) water produced in each cycle; and we also present the average concentrations calculated based on volume-averaged time integrals of the product of the effluent concentration and flowrates of Figure 2b.

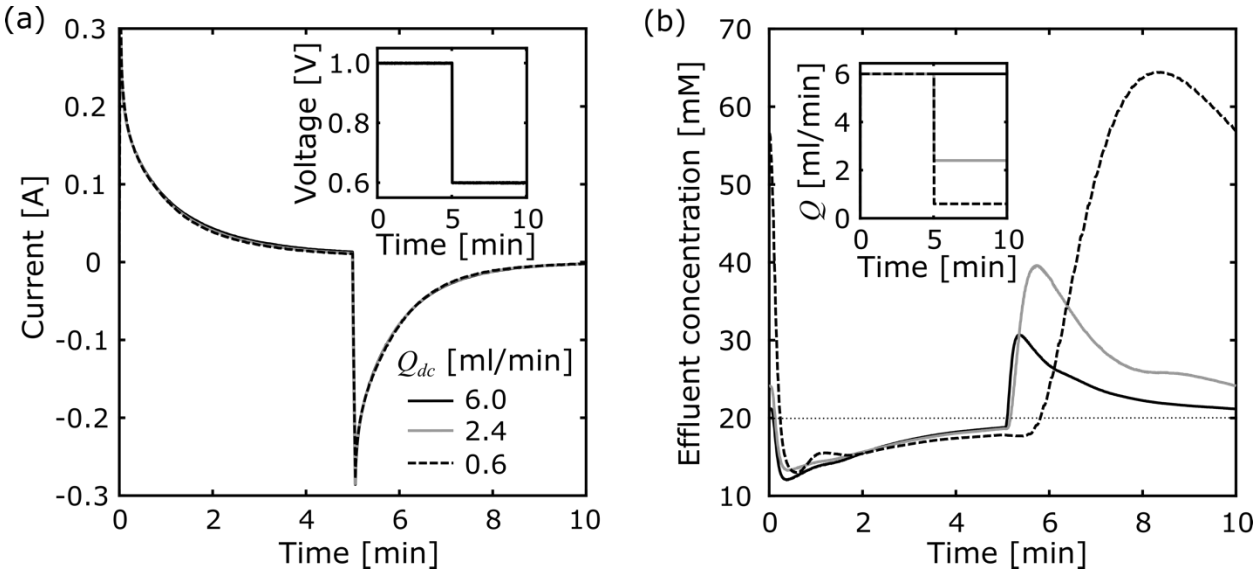

Figure 2: Measured (a) current and (b) effluent concentration as functions of time under dynamic steady state conditions for constant voltage operation between 0.6 and 1.0 V for a flowrate of 6 ml/min during charging, and discharge flowrate values (Q_{dc}) of 0.6, 2.4, and 6 ml/min. Electrical charging and discharging durations are each 5 min. The insets in (a) and (b) respectively show the forcing voltage and flowrate waveforms versus time. The current (electrical response) is insensitive to varying Q_{dc} values. On the other hand, the effluent concentration profiles show significant variations, particularly during the electrical discharge (regeneration phase).

3.1.2 Water recovery, productivity, volumetric energy consumption, and salt removal performance metrics

Figure 3 shows the performance metrics based on the experimental data of Figures 2 and S1. The figure shows water recovery, productivity, volumetric energy consumption, and average concentration reduction for discharge flowrate Q_{dc} values between 0 to 6 ml/min, and a fixed charging flowrate of 6 ml/min. Data are shown for two constant voltage operations corresponding to voltage windows of 0.2-1 V and 0.6-1 V, and charging and discharging phase durations of 300 s.

First, Figure 3a shows that measured freshwater recovery increases from about 50% to 90% as the discharge flowrate Q_{dc} decreases from 6 to near 0 ml/min. This trend is best explained by the inset of Figure 3a which plots the volume of fresh (dilute) and waste (brine) water produced per cycle. As Q_{dc} decreases, the volume of freshwater produced per cycle stays roughly constant (except very close to stop-flow discharge). However, the volume of brine generated decreases significantly, thus resulting in an increase in water recovery (fraction of freshwater produced to the total processed water; c.f. Equation (2)). We also observe in Figure 3a that water recovery values versus Q_{dc} are nearly identical for 0.2-1 V and 0.6-1 V. That is, the two voltage windows have negligible effect on water recovery. To the best of our knowledge, our work is the first systematic study to report such high values of water recovery (~90%) for CDI.

Second, Figure 3b shows that the volumetric energy consumption E_v and productivity P (shown in the inset) are each approximately constant for varying discharge flowrate Q_{dc}. As Q_{dc} is lowered to below about 0.6 ml/min (i.e. approaching stopped flow, $Q_{dc} \rightarrow 0$), productivity drops slightly (by around 10%) and the volumetric energy consumption increases slightly (by around 5%). We attribute this limiting behavior to the slight (~5%) decrease in the volume of dilute water produced (for nearly the same net energy consumption in Joules; c.f. Section 3.1.1 and inset of Figure 3a) at

stop-flow discharge conditions. We hypothesize that this effect is a result of flow mixing and dispersion inefficiencies. Note further in Figure 3b that the variation of productivity with Q_{dc} is nearly the same for 0.2-1 V and 0.6-1 V voltage windows. However, a larger voltage window (here, 0.2-1 V compared to 0.6-1 V) results in increased E_v. The increase in E_v for larger voltage windows can be attributed to higher current values and subsequently, increased resistive energy losses. See Hemmatifar et al., 2016 and Wang and Lin, 2018 for an experimental study on the effect of voltage windows and resistive losses on dissipated energy.

Third, Figure 3c shows the average concentration reduction (increase) in the dilute (brine) water as a function of Q_{dc}. Here, we observe a strong dependence on voltage window, as expected. In either voltage window, Δc_d first increases sharply, reaches a maximum near Q_{dc} = 0.6 ml/min, and is thereafter roughly constant (within about 10%) for increasing values of Q_{dc}. The inset plot shows that brine water concentration Δc_b increases, reaches a maximum (again near 0.6 ml/min) but then decreases rapidly for further increases in Q_{dc}. The larger voltage window (here, 0.2-1 V) results in higher values of Δc_d and Δc_b, which of course comes at the cost of more energy consumption (c.f. Figure 3b). Importantly we note that the variable flowrate operation with Q_{dc} value of 0.6 ml/min (corresponding to 3 ml of total feed volume or equivalently ~1 mixed reactor cell volume flowed during discharging; see Hawks et al., 2018a and Ramachandran et al., 2018b) represents a very efficient operation (c.f. Section 3.1.3 for more details). Operation with Q_{dc} of 0.6 ml/min shows that variable flowrate can be used to increase water recovery to high values (~90%) while simultaneously achieving nearly the same volumetric energy consumption, productivity, and average concentration as the conventional operation mode of constant flowrate at 6 ml/min. As an example, compared to the constant flowrate operation for 0.2-1.0 V wherein the wastewater contains 30 ml of brine at Δc_b of ~5 mM, variable flow operation with Q_{dc} of 0.6 ml/min results

in only 4 ml of brine at Δc_b of ~40 mM, while achieving approximately the same values on the other metrics.

We hypothesize that the optimal value of Q_{dc} depends on the charging mode (e.g., constant voltage or constant current as discussed in Section 3.2), charging duration, the nominal value of flowrate during charging, and dynamic charge efficiency variations, among other factors. We believe that users can perform experiments similar to those presented here with variable discharge flowrates to find the optimal value of Q_{dc} which results in high water recovery with negligible trade-offs among other performance metrics. We do not recommend operating at stop-flow during electrical discharge (i.e. Q_{dc} = 0 ml/min) as inefficiency due to flow mixing results in less than optimal performance (Hawks et al., 2018a; Ramachandran et al., 2018b). Lastly, we again highlight the aforementioned drop in Δc_d, rise in E_v, and drop in P in the region below about Q_{dc} = 0.6 ml/min.

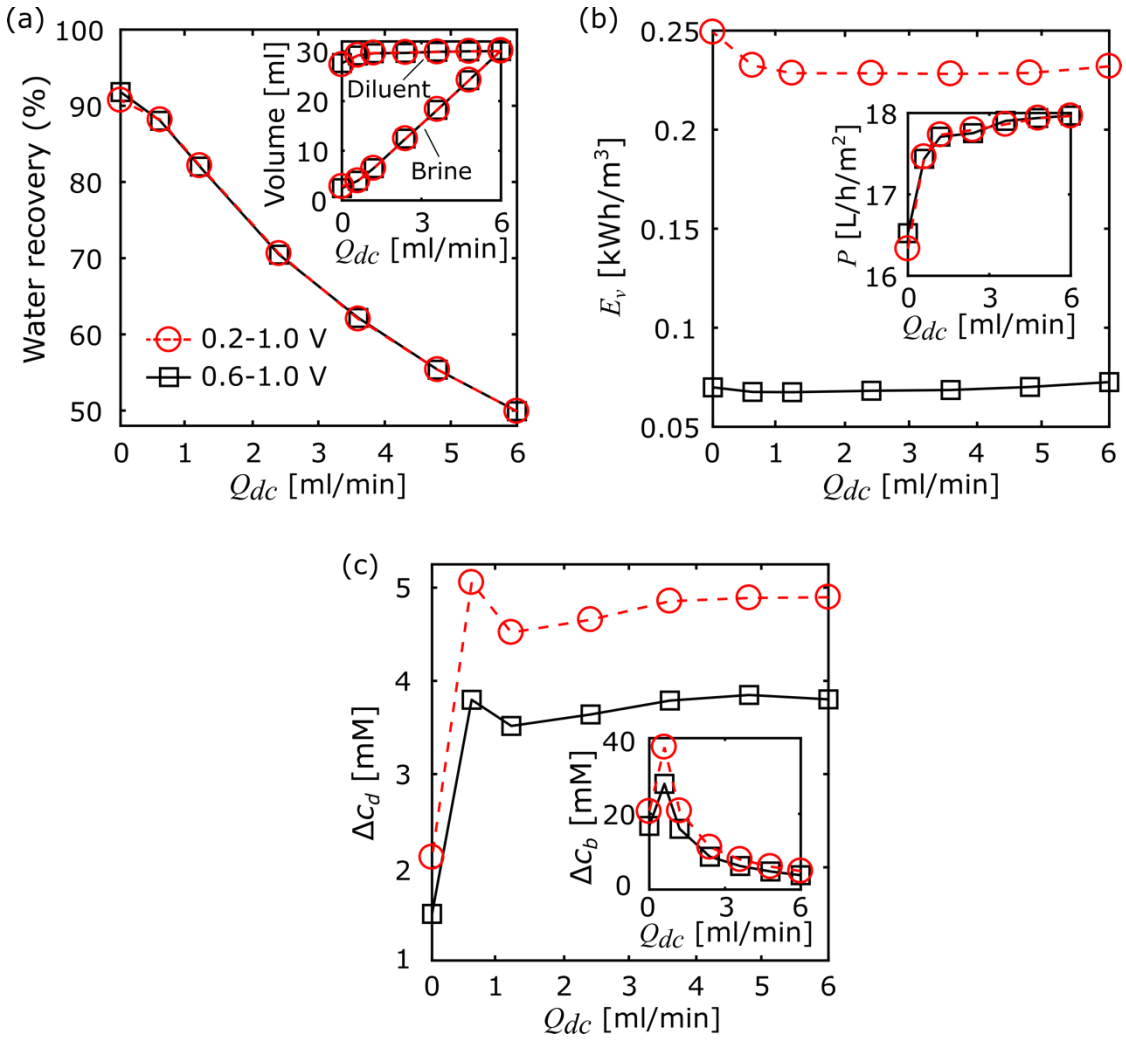

Figure 3: Measured values of (a) water recovery, (b) volumetric energy consumption, and (c) average concentration reduction in the desalted water Δc_d, for variable flowrate constant voltage operation between 0.2-1.0 V and 0.6 -1.0 V. The flowrate during charging was fixed at 6 ml/min and the flowrate during discharge (Q_{dc}) was varied between 0 to 6 ml/min. The insets in (a), (b), and (c) respectively show the volume of desalted water (and brine) produced per cycle, freshwater productivity, and average concentration increase of brine for Q_{dc} between 0 to 6 ml/min. Low values of Q_{dc} (here, at 0.6 ml/min) show freshwater recovery (~90%) with nearly the same values of productivity, Δc_d, and volumetric energy consumption compared to Q_{dc} of 6 ml/min (conventional constant flowrate operation).

3.1.3 Thermodynamic efficiency and cycle charge efficiency

Here we present a study of the effect of variable discharge flowrate Q_{dc} on thermodynamic and cycle charge efficiencies. Figure 4a shows the variation of cycle charge efficiency versus Q_{dc} for the same operating conditions as Figure 3. From Figure 4a, for fixed flowrate during charging of 6 ml/min and a fixed voltage window, we observe that charge efficiency is nearly constant for varying values of discharge flowrate between 0.6 to 6 ml/min. For Q_{dc} approaching 0 ml/min (stop-flow discharge), the charge efficiency drops significantly. As with the performance metrics discussed in Figure 3 and Section 3.1.2, we attribute this decrease in charge efficiency near stop-flow conditions ($Q_{dc} \rightarrow 0$ ml/min) to so-called flow mixing inefficiencies (Hawks et al., 2018a; Ramachandran et al., 2018b). Such inefficiencies occur when an insufficient volume of feedwater is flowed to recover the desalinated or brine solution (within the cell) at the effluent. We conclude that the variable flowrate operation introduced here maintains approximately the same charge efficiency as conventional constant flowrate operation, except obviously in the region very near $Q_{dc} = 0$ ml/min. Also note from Figure 4a that the cycle charge efficiency values for the 0.6 -1.0 V cases are overall higher than for 0.2-1.0 V cases, which is consistent with previous studies (Kim et al., 2015). The improved cycle charge efficiency for 0.6-1.0 V compared to 0.2-1.0 V is primarily due to an increased electric double layer charge efficiency at higher voltages, for nearly the same flow efficiency (Hawks et al., 2018a) and approximately same Coulombic efficiency.

Next, Figure 4b shows the thermodynamic efficiency η_{th} versus varying discharge flowrate Q_{dc} (same conditions as in Figure 3). For both 0.6-1.0 V and 0.2-1.0 V cases, we observe significant improvement in η_{th} (maximum at Q_{dc} of 0.6 ml/min) using the variable flowrate operation when compared to the conventional constant flowrate operation (Q_{dc} of 6 ml/min). We attribute these higher values of η_{th} primarily to the increased water recovery (~90%) given approximately equal

values of Δc_d (from Equations (8) and (7)) and E_v. Lastly, we also observe from Figure 4b that thermodynamic efficiency is overall higher for the 0.6-1.0 V cases when compared to 0.2-1.0 V cases, similar to the trend in Figure 4a for charge efficiency.

Thus, at near-optimal performance for CV variable flowrate operation, we find an improvement in freshwater recovery to ~90% (from 50%) for nearly the same productivity, volumetric energy consumption, and average concentration reduction (~ 4 to 5 mM removal from 20 mM feed water) in the freshwater when compared to the conventional constant flowrate operation. Furthermore, the variable flowrate operation also increases the thermodynamic efficiency significantly (by ~2 to 3-fold) at near-optimal operation. We note here that this increase in thermodynamic efficiency is primarily due to an increase in the Gibbs free energy of separation process, ΔG_{sep} (due to increased water recovery for nearly the same Δc_d), (see Hemmatifar et al., 2018) and for nearly the same energy consumption (c.f. Figure 3b). These results clearly highlight the benefits and importance of using a low (but greater than zero) flowrate during electrical discharge for desalination using CDI. In the next section, we demonstrate that variable flowrate operation can also be used to improve constant current operation.

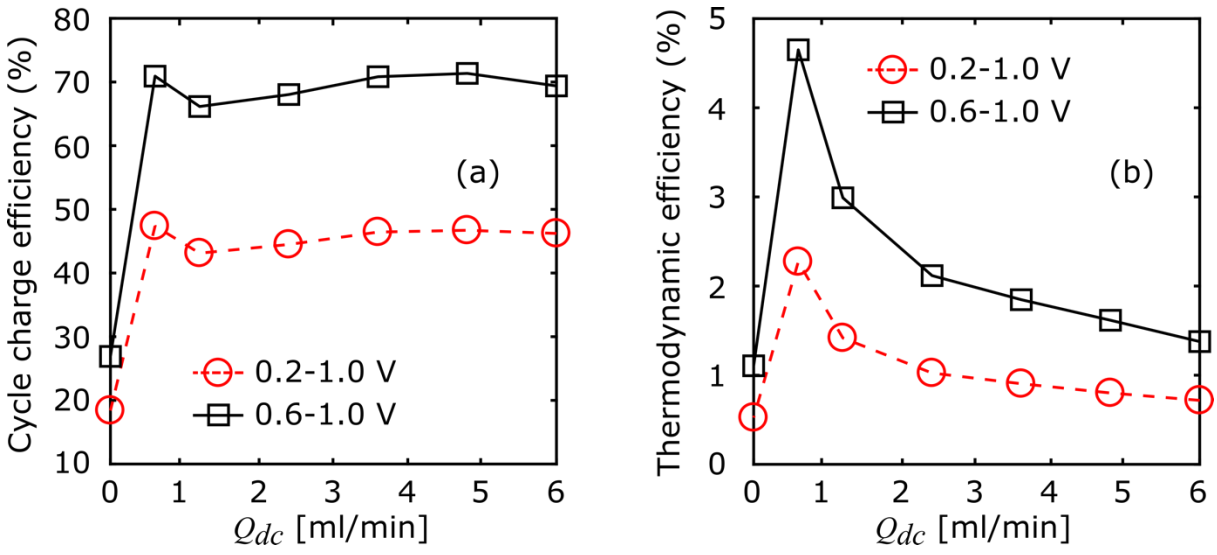

Figure 4: Measured values of (a) cycle-averaged charge efficiency Λ, and (b) thermodynamic efficiency η_{th} for the same operational conditions as Figure 3. Note that charge efficiency for a given voltage window is relatively constant for varying values of Q_{dc}, except near Q_{dc} = 0 ml/min (stop-flow discharge). Further, thermodynamic efficiency can increase from about 1.4 to 4.7% (typically, by ~2 to 3-fold) for operation at low values of Q_{dc} (e.g. here at 0.6 ml/min) when compared to conventional constant flow operation (i.e. Q_{dc} of 6 ml/min).

3.2 Constant current electrical charging-discharging with variable flowrate

We here discuss results from a series of constant current (CC) charge-discharge experiments performed at a fixed nominal flowrate value of 3 ml/min during charging, and varying flowrate values of 3, 2.4, 1.8, 1.2, 0.6, 0.3, and 0 ml/min during discharging. We studied this operation for two values of charging and discharging currents of $\pm$25 and $\pm$50 mA, between 0.2-1.0 V.

3.2.1 Voltage and effluent concentration response

Figures 5a and 5b show the voltage and effluent concentration responses respectively for constant current (CC) operation at 50 mA and flowrate of 3 ml/min during charging, and discharge flowrates of 3, 1.8, and 0.6 ml/min. The insets in Figures 5a and 5b show the input current and flowrate waveforms, respectively.

Figure 5a shows that the time variation of voltage response is nearly the same for different values of flowrate during discharge Q_{dc} between 0.6 to 3 ml/min. The charging duration decreases only slightly (~10 s, or less than 2% change) for values of Q_{dc} lower than 3 ml/min (which corresponds to the conventional constant flowrate operation). Since the temporal variations of current and voltage are nearly independent of discharge flowrate, the net electrical energy consumption and electrical charge transferred per cycle are accordingly approximately equal across a wide range of

Q_{dc} values between 0 to 3 ml/min (see Figure S4). Recall we observed a similar trend for the constant voltage operation where the electrical responses (formerly current vs. time) were also only weakly dependent on discharge flowrate variations (c.f. Section 3.1.1). Refer to Figure S3 for further effluent voltage response data at Q_{dc} values of 2.4, 1.2, and 0 ml/min for 50 mA CC operation, and for the aforementioned Q_{dc} values with 25 mA CC charging-discharging.

Next, Figure 5b shows that the main effect of lowering discharge flowrate on effluent concentration response versus time is to increase the concentration of brine during electrical discharge. During the charging phase, the effluent concentration profiles are very similar for varying Q_{dc} values between 0.6 to 3 ml/min. Further, for low (but non-zero) values of Q_{dc} (e.g. here, 0.6 ml/min), the quasi-steady state value of effluent concentration during charging drops to a slightly lower value than for a constant flowrate case (i.e. Q_{dc} of 3 ml/min). As with the constant voltage case, that the constant current data show that a reduction in Q_{dc} causes time delays in the crossover point where effluent concentration crosses feedwater concentration during both charging and discharging. Again, the most significant delays are observed during the discharge phase. In the next subsection, we use the effluent concentration, current, and voltage profiles to explore the variation of the performance metrics due to varying discharge flowrates.

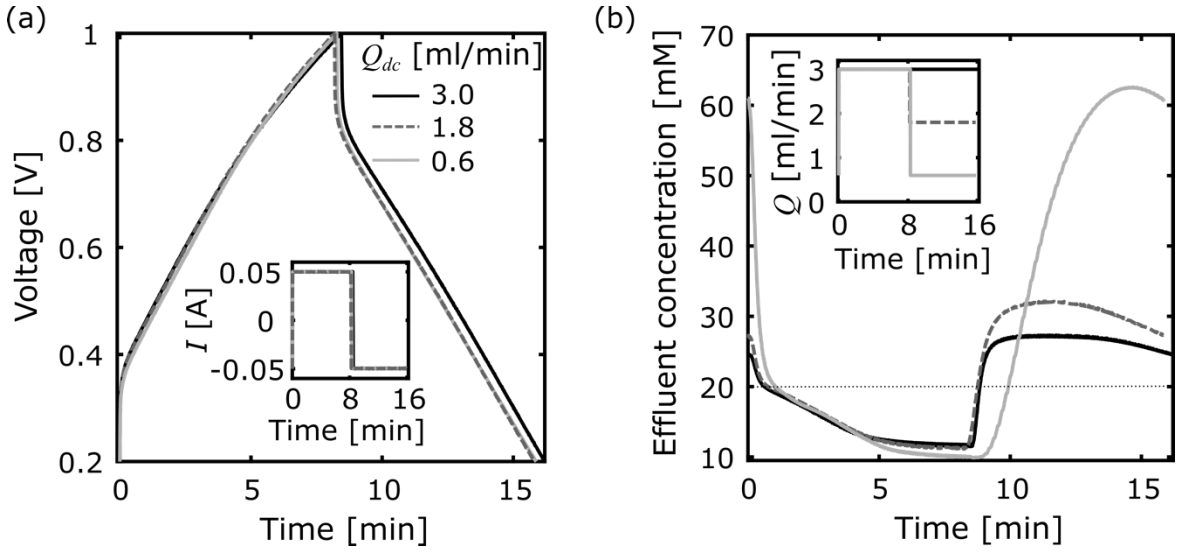

Figure 5: Measured time variation of (a) voltage, and (b) effluent concentration under dynamic steady state conditions for constant current charge-discharge operation at ±50 mA for a flowrate of 3 ml/min during charging, and for discharge flowrate values (Q_{dc}) of 0.6, 1.8, and 3 ml/min. The insets in (a) and (b) respectively show the forcing current and flowrate waveforms versus time. Note that the voltage response is less sensitive to varying Q_{dc} values. However, as in Figure 2, the effluent concentration profiles show significant variations (mainly during the electrical discharge/salt regeneration phase) for varying discharge flowrates.

3.2.2 Water recovery, productivity, volumetric energy consumption, and salt removal performance metrics

Figure 6 shows the effect of varying discharge flowrate on the performance metrics for the data of Figures 5 and S3. Shown are water recovery, productivity, volumetric energy consumption, and average concentration reduction for constant current (CC) operation for discharge flowrate values between 0 to 3 ml/min, and fixed charging flowrate of 3 ml/min. Data are shown for CC charge-discharge currents of ±25 and ±50 mA, and for a voltage window of 0.2-1 V.

First, from Figure 6a, we observe that as Q_{dc} is lowered from 3 to 0.6 ml/min, water recovery increases from ~50% to ~78% and ~84% for 50 mA and 25 mA, respectively. As Q_{dc} is further decreased below 0.6 ml/min, water recovery drops to ~68%. These trends can be understood from the data of inset Figure 6a which plots the variation of the freshwater and brine volumes generated per cycle as a function of Q_{dc}. From the inset in Figure 6a, we note that the volume of freshwater generated per cycle V_d is nearly constant as Q_{dc} is lowered from 3 ml/min to 0.6 ml/min. The freshwater volume then drops significantly for Q_{dc} lower than 0.6 ml/min. On the other hand, we see the volume of brine V_b generated per cycle drops approximately linearly as Q_{dc} is lowered from 3 to 0.6 ml/min. Lowering Q_{dc} below 0.6 ml/min results in a slight increase in V_b. These variations each contribute to the increase in water recovery observed in the main plot of Figure 6a, and the dominant effect is the decrease in the brine volume (for nearly the same freshwater volume) produced per CDI cycle. We hypothesize that the changes in trends for values of Q_{dc} lower than 0.6 ml/min are due to dispersion and mixing inefficiencies, as these become more important for low feed volumes (compared to the effective mixed reactor volume) (Hawks et al., 2018a; Ramachandran et al., 2018b). Note that these general observations for the variable flowrate and CC operation are very similar to those reported above for the constant voltage cases (c.f. Section 3.1.2). We also highlight that our work is the first to report such high values of water recovery (~80-85%) for CDI with constant current operation. Comparing CC and CV operation, we observe a slightly lower maximum water recovery achieved by CC operation compared to CV operation (maximum water recovery of ~90%) under the variable flowrate scheme. We hypothesize that this is due to the differences in salt removal/regeneration rates between CC and CV modes.

Second, the data of Figure 6b show that volumetric energy consumption E_v values are nearly constant (for a given CC value) as Q_{dc} is lowered from 3 to 0.6 ml/min, For Q_{dc} lower than

0.6 ml/min, E_v increases by ~30%. Likewise, productivity P (shown in the inset of Figure 6b) is nearly constant as Q_{dc} is lowered from 3 to 0.6 ml/min, but P decreases by ~20% for Q_{dc} lower than 0.6 ml/min. The volume of freshwater V_d produced per cycle in nearly constant for $Q_{dc} \gtrsim 0.6$ ml/min, but V_d decreases as $Q_{dc} \to 0$ (c.f. inset of Figure 6a), likely a result of mixing inefficiencies. At the same time, the total energy consumption (in Joules) is insensitive to variations in Q_{dc} (c.f. Section 3.2.1 and Figure S4). Accordingly, Figure 6b shows that the volumetric energy cost is overall higher for higher currents (e.g. here, for 50 mA). We attribute this to the increased resistive energy loss of higher currents accompanied by lower volume of freshwater produced (due to shorter charging durations for a given voltage window and nominal flowrate). Productivity values, on the other hand, are similar for the 25 and 50 mA cases since P mainly depends on the flowrate during charging, which is equal to 3 ml/min for both the CC cases.

Third, Figure 6c shows the average concentration reduction in the dilute water Δc_d is nearly constant (with a slight increase) as Q_{dc} is lowered from 3 to 0.6 ml/min, and Δc_d reaches a maximum at Q_{dc} of 0.6 ml/min. For further decreases in Q_{dc}, Δc_d decreases by about 25%. We hypothesize that the decrease in Δc_d as $Q_{dc} \to 0$ ml/min is due to flow mixing inefficiencies (Hawks et al., 2018a; Ramachandran et al., 2018b). The inset in Figure 6c shows the corresponding increase in concentration of wastewater brine Δc_b versus Q_{dc}. Similar to Δc_d, we observe from the inset that Δc_b increases by 3 to 4-fold as Q_{dc} is lowered from 3 to 0.6 ml/min. Δc_b reaches a maximum at Q_{dc} of 0.6 ml/min, and Δc_b decreases as Q_{dc} is lowered further. Further, Figure 6c shows for a given voltage window and nominal flowrate, a higher current (here, 50 mA) results in a higher Δc_d and Δc_b values overall.

Hence, from the performance metrics analyzed in Figure 6, we note that there exists an "optimal" value of Q_{dc} (greater than 0, but much lower than the nominal flowrate value of 3 ml/min) for

which the productivity, volumetric energy consumption, and Δc_d are nearly constant or better than the corresponding constant flowrate operation, while water recovery is very high (~80-85%) compared to the conventional value of 50%. Operation at optimal Q_{dc} using the variable flowrate method changes primarily the nature of the wastewater produced in a CDI cycle. That is, variable flowrate operation results in a highly concentrated brine with very low volume, but has negligible effect on freshwater quality, production rate, and the energetics of the process. These observations for constant current variable flowrate operation are similar to those discussed earlier for constant voltage with variable flowrate (c.f. Section 3.1.2), thus highlighting the general applicability and advantages of the variable flowrate operation.

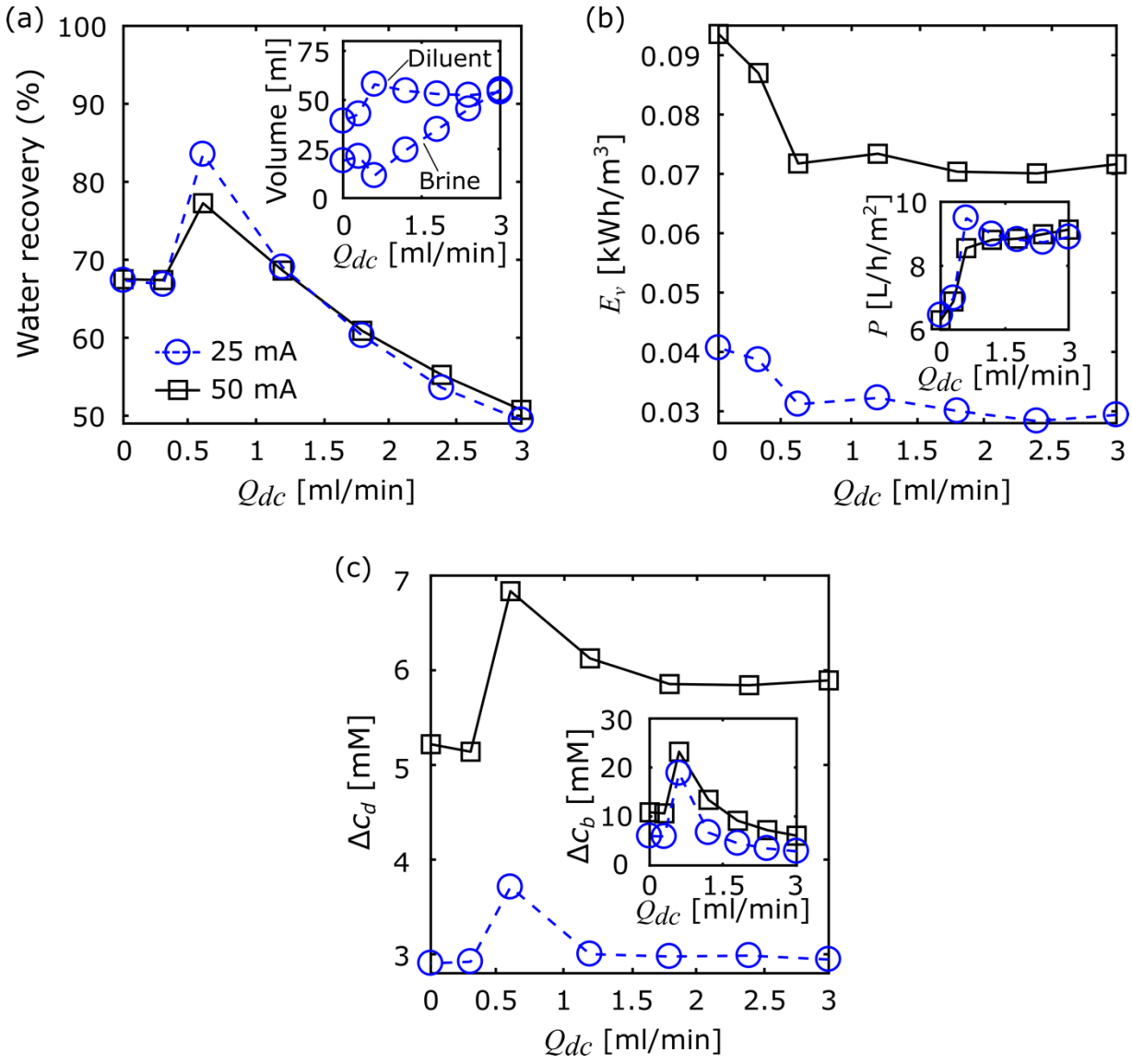

Figure 6: Measured values of performance metrics - (a) freshwater recovery, (b) volumetric energy consumption, and (c) average concentration reduction in the desalted water Δc_d, for variable flowrate constant current charge-discharge operation at 25 and 50 mA between 0.2-1.0 V. The flowrate during charging was fixed at 3 ml/min and the flowrate during discharge (Q_{dc}) was varied between 0 to 3 ml/min. The inset in (a) shows the volumes of desalted and brine water generated per cycle for the 25 mA cases (refer to Figure S5 for corresponding plots for the 50 mA cases). The insets in (b) and (c) respectively show the freshwater productivity and average

concentration of brine (waste) water versus varying Q_{dc} between 0 to 3 ml/min. High freshwater recovery (~80-85%) is achieved for Q_{dc} near 0.6 ml/min while simultaneously achieving nearly the same (or better) values of productivity, Δc_d, and volumetric energy consumption compared to Q_{dc} of 3 ml/min (conventional constant flowrate operation).

3.2.3 Thermodynamic and cycle charge efficiency

Figures 7a and 7b respectively show the cycle charge efficiency and thermodynamic efficiency for the constant current variable flowrate operation (same operating conditions as in Figure 6). Data are shown for two values of CC charge-discharge currents of 25 and 50 mA, flowrate during charging of 3 ml/min, and discharge flowrate varying between 0 to 3 ml/min.

From Figure 7a, for both 25 and 50 mA cases, as Q_{dc} is lowered from 3 to 0.6 ml/min, cycle charge efficiency Λ is nearly constant, and then Λ increases and reaches a maximum near Q_{dc} of 0.6 ml/min. When Q_{dc} is further lowered, Λ drops sharply. We hypothesize that the drop in Λ as $Q_{dc} \rightarrow 0$ ml/min is due to flow mixing inefficiencies (c.f. Section 3.2.2). Importantly, we note here that at the "optimal" value of Q_{dc} (here, at 0.6 ml/min), the cycle charge efficiency of the variable flowrate operation is at least equal to (or higher) than a constant flowrate operation (i.e. for Q_{dc} of 3 ml/min).

From Figure 7b, thermodynamic efficiency η_{th} increases rapidly as Q_{dc} is lowered from 3 to 0.6 ml/min, reaches a maximum at the "optimal" value of Q_{dc} (here, 0.6 ml/min), and then decreases as Q_{dc} is lowered in a manner similar to cycle charge efficiency. Note that at optimal performance, η_{th} is ~8% — a factor ~3-fold higher than the conventional constant flowrate operation (i.e. for Q_{dc} of 3 ml/min) for which η_{th} ~2-3%. This, we hypothesize, is mainly a result of the much higher water recovery (~85%) achieved by the variable flowrate operation (for nearly

455 the same or better Δc_d) when compared to the conventional constant flowrate operation (water
456 recovery of ~50%). We note here that the overall observations for the efficiency measures (η_{th}
457 and Λ) for a constant current variable flowrate operation resonate well with the corresponding
458 constant voltage counterpart (c.f. Section 3.1.3), again emphasizing the advantages of the variable
459 flowrate operation for CDI, in general.

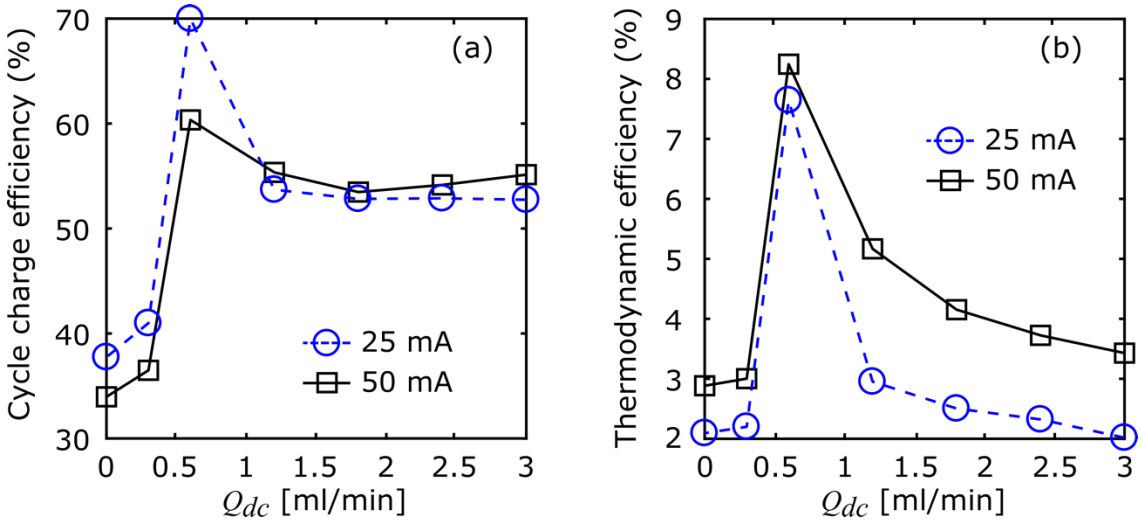

460

461 **Figure 7**: Measured values of (a) cycle-averaged charge efficiency and (b) thermodynamic
462 efficiency for the same constant current variable flowrate operation as in Figure 6. For each CC
463 case, as Q_{dc} is lowered from 3 to 0 ml/min, charge efficiency is first nearly constant, then increases
464 and reaches maximum (here at 0.6 ml/min), and finally decreases for Q_{dc} approaching 0 ml/min
465 (stopped flow). Furthermore, at the "optimal" value of Q_{dc} (here at 0.6 ml/min), the thermodynamic
466 efficiency η_{th} is also maximum, equal to ~8%; note that this is ~2 to 3-fold the corresponding η_{th}
467 value (equal to ~ 2-3%) of a constant flowrate operation (i.e. Q_{dc} of 3 ml/min).

468 **4. Summary and conclusions**

469 We performed an experimental study of a variable flowrate operation for CDI which involves
470 flowing at a nominal flow rate during electrical charging and a lower flowrate during electrical

discharging. We applied this operating method to both constant current and constant voltage electrical charge-discharge schemes. We systematically studied the effect of variable flowrate operation on the performance and efficiency of our custom-built CDI cell. For the first time, we systematically show that freshwater recovery for conventional CDI can be increased to as high as 85-90% in a single-pass desalination cycle under realistic salt removal conditions. In addition to high water recovery, we demonstrated the same performance in volumetric energy consumption, productivity, and average concentration reduction in the freshwater using the variable flowrate operation (at near-optimal performance) when compared to the conventional constant flowrate operation. Moreover, the thermodynamic efficiency of the desalination process was shown to increase by 2 to 3-fold using the variable flowrate method compared to constant flow operation, under similar conditions. This was achieved primarily by increasing the Gibbs free energy of separation by improving water recovery for nearly the same salt removal and energy consumption.

We hypothesize that the variable flowrate scheme introduced in this work can be easily implemented in a wide range of existing CDI systems for improved overall performance. We caution that overly low flowrates during discharge (i.e. when operated at less than optimal flowrate) can result in mixing losses due to inefficient recovery of fresh or concentrated water at the effluent from within the cell. Thus, to avoid this sub-optimal operating condition, we recommend the following procedure to find near-optimal values of discharge flowrate for high water recovery operation irrespective of the electrical charging method. First, the nominal flowrate during electrical charging can be determined by the desired productivity and average concentration reduction, assuming a conventional constant flowrate operation. Next, the flowrate during discharge can be decreased (as demonstrated in Sections 3.1 and 3.2) to find the “optimal” condition for which the performance metrics. This optimal condition is characterized by an

operating point wherein water recovery is optimized while achieving volumetric energy consumption, productivity, and average concentration reductions approximately equal to those of the typical 50% water recovery case. We hypothesize that the optimal value of discharge flowrate depends on the charging modes, effective mixed-reactor volume, dispersion in the header, nominal flowrate during charging, among many other factors, and thus needs to be determined individually for each baseline operating condition.

We further note that the volumes of dilute and brine solutions produced per CDI cycle do not simply scale with the amount of feed volume processed during electrical charging and discharging respectively. We believe that the deviation from this scaling is due to the coupled physics of mixed-reactor salt removal (fluid flow) and circuit (electrical) dynamics for CDI (Hawks et al., 2018a; Ramachandran et al., 2018a), together with the effects of dispersion and mixing at low flowrates.

Acknowledgements

A.R. gratefully acknowledges the support from the Bio-X Bowes Fellowship of Stanford University. We gratefully acknowledge funding from the California Energy Commission grant ECP-16-014. Work at LLNL was performed under the auspices of the US DOE by LLNL under Contract DE-AC52-07NA27344.

References

Anderson, M.A., Cudero, A.L., Palma, J., 2010. Capacitive deionization as an electrochemical means of saving energy and delivering clean water. Comparison to present desalination

practices: Will it compete? Electrochim. Acta 55, 3845–3856. https://doi.org/10.1016/J.ELECTACTA.2010.02.012

Biesheuvel, P.M., 2009. Thermodynamic cycle analysis for capacitive deionization. J. Colloid Interface Sci. https://doi.org/10.1016/j.jcis.2008.12.018

Biesheuvel, P.M., van der Wal, A., 2010. Membrane capacitive deionization. J. Memb. Sci. https://doi.org/10.1016/j.memsci.2009.09.043

Choi, J.-H., 2015. Comparison of constant voltage (CV) and constant current (CC) operation in the membrane capacitive deionisation process. Desalin. Water Treat. 56, 921–928. https://doi.org/10.1080/19443994.2014.942379

Dlugolecki, P., Connorton-Spragg, A., Carlos, C., 2016. Application of Membrane Capacitive Deionization Technology in cooling towers. Ultrapure Water.

García-Quismondo, E., Santos, C., Lado, J., Palma, J., Anderson, M.A., 2013. Optimizing the energy efficiency of capacitive deionization reactors working under real-world conditions. Environ. Sci. Technol. https://doi.org/10.1021/es4021603

García-Quismondo, E., Santos, C., Soria, J., Palma, J., Anderson, M.A., 2016. New Operational Modes to Increase Energy Efficiency in Capacitive Deionization Systems. Environ. Sci. Technol. https://doi.org/10.1021/acs.est.5b05379

Hawks, S.A., Knipe, J.M., Campbell, P.G., Loeb, C.K., Hubert, M.A., Santiago, J.G., Stadermann, M., 2018a. Quantifying the flow efficiency in constant-current capacitive deionization. Water Res. 129, 327–336. https://doi.org/10.1016/j.watres.2017.11.025

Hawks, S.A., Ramachandran, A., Campbell, P.G., Suss, M.E., Biesheuvel, P.M., Santiago, J.G.,

Stadermann, M., 2018b. Performance Metrics for the Objective Assessment of Capacitive Deionization Systems.

Hemmatifar, A., Palko, J.W., Stadermann, M., Santiago, J.G., 2016. Energy breakdown in capacitive deionization. Water Res. https://doi.org/10.1016/j.watres.2016.08.020

Hemmatifar, A., Ramachandran, A., Liu, K., Oyarzun, D.I., Bazant, M.Z., Santiago, J.G., 2018. Thermodynamics of Ion Separation by Electrosorption.

Jande, Y.A.C., Kim, W.S., 2013. Desalination using capacitive deionization at constant current. Desalination 329, 29–34. https://doi.org/10.1016/j.desal.2013.08.023

Kang, J., Kim, T., Jo, K., Yoon, J., 2014. Comparison of salt adsorption capacity and energy consumption between constant current and constant voltage operation in capacitive deionization. Desalination 352, 52–57. https://doi.org/10.1016/j.desal.2014.08.009

Kim, T., Dykstra, J.E., Porada, S., van der Wal, A., Yoon, J., Biesheuvel, P.M., 2015. Enhanced charge efficiency and reduced energy use in capacitive deionization by increasing the discharge voltage. J. Colloid Interface Sci. https://doi.org/10.1016/j.jcis.2014.08.041

Oren, Y., 2008. Capacitive deionization (CDI) for desalination and water treatment — past, present and future (a review). Desalination 228, 10–29. https://doi.org/10.1016/J.DESAL.2007.08.005

Porada, S., Zhao, R., van der Wal, A., Presser, V., Biesheuvel, P.M., 2013. Review on the science and technology of water desalination by capacitive deionization. Prog. Mater. Sci. 58, 1388–1442. https://doi.org/10.1016/J.PMATSCI.2013.03.005

Qu, Y., Campbell, P.G., Gu, L., Knipe, J.M., Dzenitis, E., Santiago, J.G., Stadermann, M., 2016.

Energy consumption analysis of constant voltage and constant current operations in capacitive deionization. Desalination 400, 18–24. https://doi.org/10.1016/j.desal.2016.09.014

Ramachandran, A., Hawks, S.A., Stadermann, M., Santiago, J.G., 2018a. Frequency analysis and resonant operation for efficient capacitive deionization.

Ramachandran, A., Hemmatifar, A., Hawks, S.A., Stadermann, M., Santiago, J.G., 2018b. Self similarities in desalination dynamics and performance using capacitive deionization. Water Res. https://doi.org/10.1016/J.WATRES.2018.04.042

Shang, X., Cusick, R.D., Smith, K.C., 2017. A Combined Modeling and Experimental Study Assessing the Impact of Fluid Pulsation on Charge and Energy Efficiency in Capacitive Deionization. J. Electrochem. Soc. 164, E536–E547. https://doi.org/10.1149/2.0841714jes

Wang, L., Biesheuvel, P.M., Lin, S., 2018. Reversible thermodynamic cycle analysis for capacitive deionization with modified Donnan model. J. Colloid Interface Sci. https://doi.org/10.1016/j.jcis.2017.10.060

Wang, L., Lin, S., 2018. Membrane Capacitive Deionization with Constant Current vs Constant Voltage Charging: Which Is Better? Environ. Sci. Technol. https://doi.org/10.1021/acs.est.7b06064

Zhao, R., Biesheuvel, P.M., van der Wal, A., 2012. Energy consumption and constant current operation in membrane capacitive deionization. Energy Environ. Sci. 5, 9520. https://doi.org/10.1039/c2ee21737f

Supplementary Information for

High water recovery and improved thermodynamic efficiency for capacitive deionization using variable flowrate operation

Ashwin Ramachandran,[a] Diego I. Oyarzun,[b] Steven A. Hawks,[c] Michael Stadermann,[c] and Juan G. Santiago [b,*]

[a] Department of Aeronautics & Astronautics, Stanford University, Stanford, California 94305, United States

[b] Department of Mechanical Engineering, Stanford University, Stanford, California 94305, United States

[c] Lawrence Livermore National Laboratory, 7000 East Avenue, Livermore, CA, 94550, United States

* To whom correspondence should be addressed. E-mail: juan.santiago@stanford.edu

Contents

1. Effluent concentration and current response versus time for constant voltage and variable flowrate operation

2. Charge transferred and energy consumption for constant voltage and variable flowrate operation

3. Effluent concentration and voltage response versus time for constant current and variable flowrate operation

4. Charge transferred and energy consumption for constant current and variable flowrate operation

5. Volume of dilute and brine solutions produced per cycle for constant current and variable flowrate operation

1. Effluent concentration and current response versus time for constant voltage and variable flowrate operation

Figure S1 shows raw experimental measurements for current and effluent concentration versus time for each of two applied voltage ranges. The start of the charging or discharge phases are fixed at 5 and 10 min, respectively.

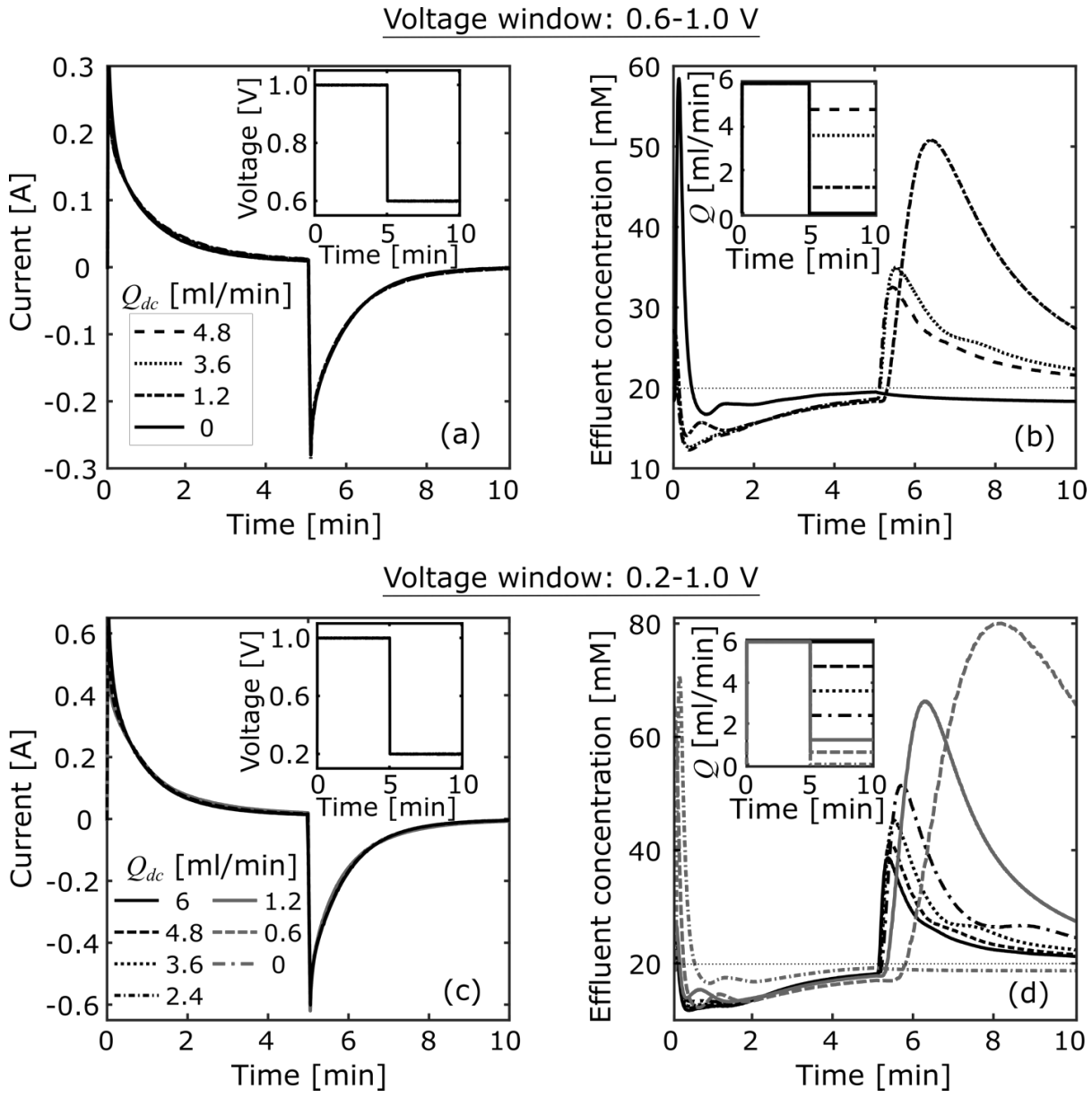

Figure S1: Measured (a) current and (b) effluent concentration as functions of time under dynamic steady state conditions for constant voltage operation between 0.6 and 1.0 V for a flowrate of 6 ml/min during charging, and discharge flowrate values (Q_{dc}) of 0, 1.2, 3.6, and 4.8 ml/min.

Measured time variation of (c) current and (d) effluent concentration under dynamic steady state conditions for constant voltage operation between 0.2 and 1.0 V for a flowrate of 6 ml/min during charging, and discharge flowrate values (Q_{dc}) of 0, 0.6, 1.2, 2.4, 3.6, 4.8 and 6.0 ml/min. Electrical charging and discharging phase durations are each 5 min. The insets in (a) and (c) show the forcing voltage versus time, and the insets in (b) and (d) show the time variation of flowrate. Note that the electrical response is nearly identical for different values of discharge flowrates.

2. Charge transferred and energy consumption for constant voltage and variable flowrate operation

Figure S2a shows measured net electrical charge input and output for each of the two voltage windows. Figure S2b shows the corresponding values of energy consumption and recovery. These results correspond to the experimental results presented in Figures 2 and S1. Note that for a given voltage window, the electrical charge input and output, and energy consumed and recovered, are nearly the same for varying discharge flowrate values. This highlights that the electrical response of CDI is less sensitive to variation in flowrates.

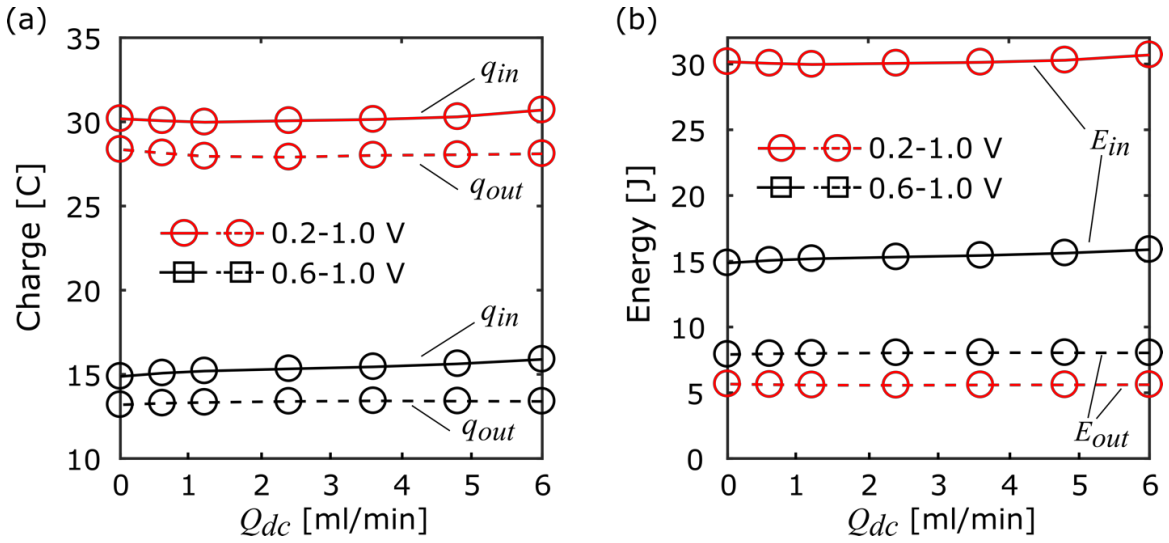

Figure S2: Measured (a) electrical charge input (q_{in}) and output (q_{out}) in Coulombs, and (b) energy consumption (E_{in}) and recovery (E_{out}) in Joules, versus discharge flowrate for the variable flowrate and constant voltage operation between 0.2-1.0 V and 0.6-1.0 V. The flowrate during charging was fixed at 6 ml/min and the flowrate during discharge (Q_{dc}) was varied between 0 to 6 ml/min.

3. Effluent concentration and voltage response versus time for constant current and variable flowrate operation

Figure S3 shows raw experimental measurements for voltage and effluent concentration versus time for two constant current operations subject to the same voltage window of 0.2-1.0 V. The start of the charging or discharge phases are determined by the times at which the measured voltages reached the minimum and maximum voltages of the window, respectively.

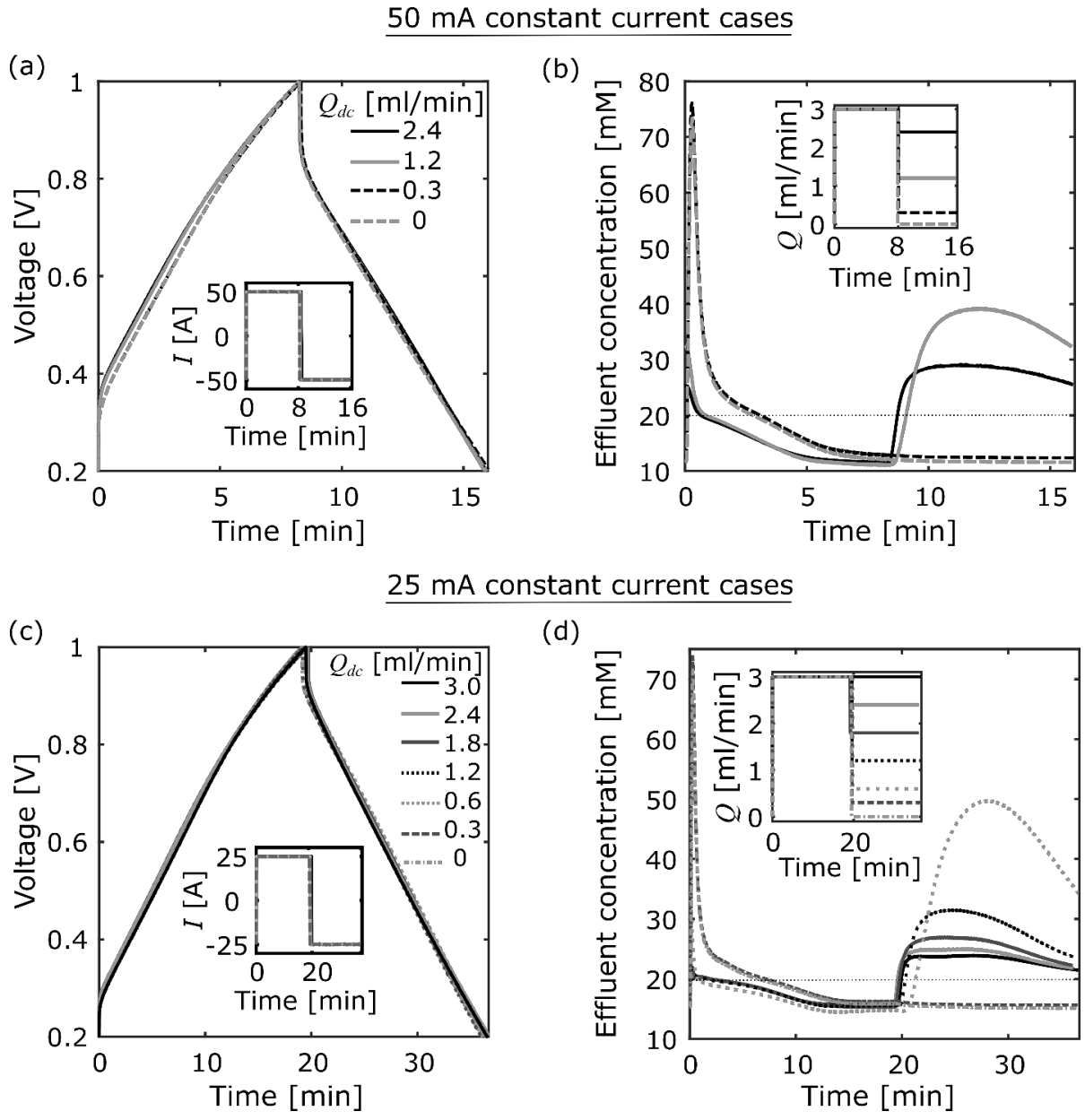

Figure S3: Measured time variation of (a) voltage, and (b) effluent concentration under dynamic steady state conditions for constant current charge-discharge operation at ±50 mA for a flowrate

of 3 ml/min during charging, and for discharge flowrate values (Q_{dc}) of 0, 0.3, 1.2, and 2.4 ml/min. Measured (c) voltage, and (b) effluent concentration versus time under dynamic steady state conditions for constant current charge-discharge operation at ±25 mA for a flowrate of 3 ml/min during charging, and for discharge flowrate values (Q_{dc}) of 0, 0.3, 0.6, 1.2, 1.8, 2.4, and 3.0 ml/min. The insets in (a) and (c) show the time variation of forcing current, and the insets in (c) and (d) show flowrate waveforms versus time.

4. Charge transferred and energy consumption for constant current and variable flowrate operation

Figure S4a shows measured net electrical charge input and output for each of the two applied current values. Figure S2b shows the corresponding values of energy consumption and recovery. These results correspond to the experimental results presented in in Figures 5 and S3. Note that for a given constant current operation, the electrical charge input and output, and energy consumed and recovered, are nearly the same (less than 5% variation) for varying discharge flowrate values.

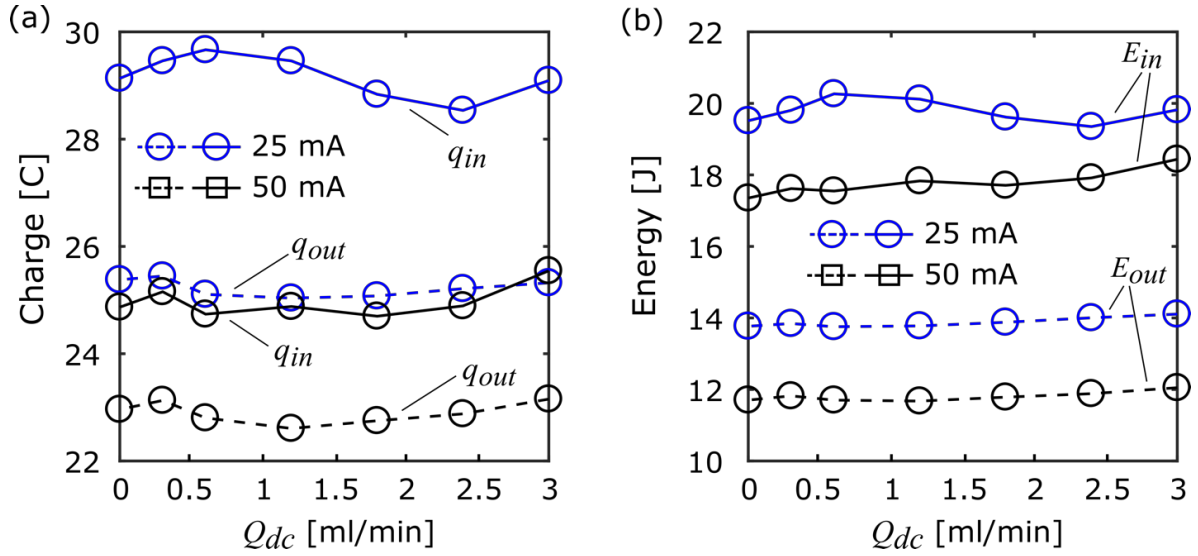

Figure S4: Measured (a) charge input (q_{in}) and output (q_{out}) in Coulombs, and (b) energy consumption (E_{in}) and recovery (E_{out}) in Joules, versus discharge flowrate for the variable flowrate and constant current operation at 25 and 50 mA between 0.2-1.0 V. The flowrate during charging was fixed at 3 ml/min and the flowrate during discharge (Q_{dc}) was varied between 0 to 3 ml/min.

5. Volume of dilute and brine solutions produced per cycle for constant current and variable flowrate operation

Lastly, Figure S5 shows measured volumes of diluent (desalted water output) and output brine per CDI cycle. These data correspond to the experimental results presented in Figures 5 and S3.

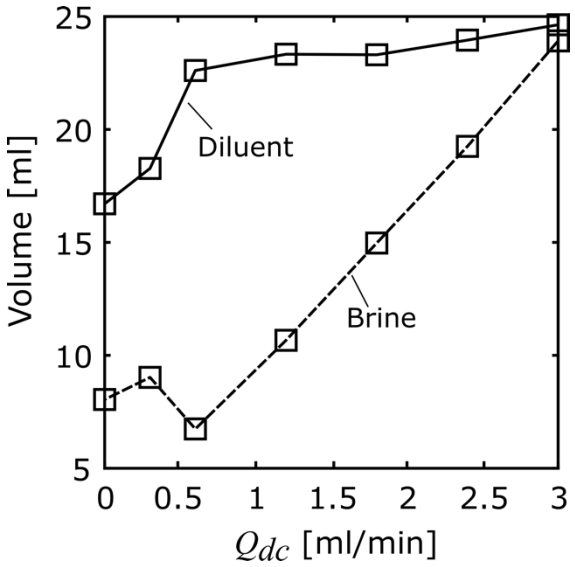

Figure S5: Measured volumes of desalted and brine water generated per cycle versus discharge flowrate for constant current and variable flowrate operation at 50 mA. The flowrate during charging was fixed at 3 ml/min and the flowrate during discharge (Q_{dc}) was varied between 0 to 3 ml/min. See inset of Figure 6a for data corresponding to operation at 25 mA.

Supplementary Information for

High water recovery and improved thermodynamic efficiency for capacitive deionization using variable flowrate operation

Ashwin Ramachandran,[a] Diego I. Oyarzun,[b] Steven A. Hawks,[c] Michael Stadermann,[c] and Juan G. Santiago [b,*]

[a] Department of Aeronautics & Astronautics, Stanford University, Stanford, California 94305, United States

[b] Department of Mechanical Engineering, Stanford University, Stanford, California 94305, United States

[c] Lawrence Livermore National Laboratory, 7000 East Avenue, Livermore, CA, 94550, United States

* To whom correspondence should be addressed. E-mail: juan.santiago@stanford.edu

Contents

1. Effluent concentration and current response versus time for constant voltage and variable flowrate operation

2. Charge transferred and energy consumption for constant voltage and variable flowrate operation

3. Effluent concentration and voltage response versus time for constant current and variable flowrate operation

4. Charge transferred and energy consumption for constant current and variable flowrate operation

5. Volume of dilute and brine solutions produced per cycle for constant current and variable flowrate operation

1. Effluent concentration and current response versus time for constant voltage and variable flowrate operation

Figure S1 shows raw experimental measurements for current and effluent concentration versus time for each of two applied voltage ranges. The start of the charging or discharge phases are fixed at 5 and 10 min, respectively.

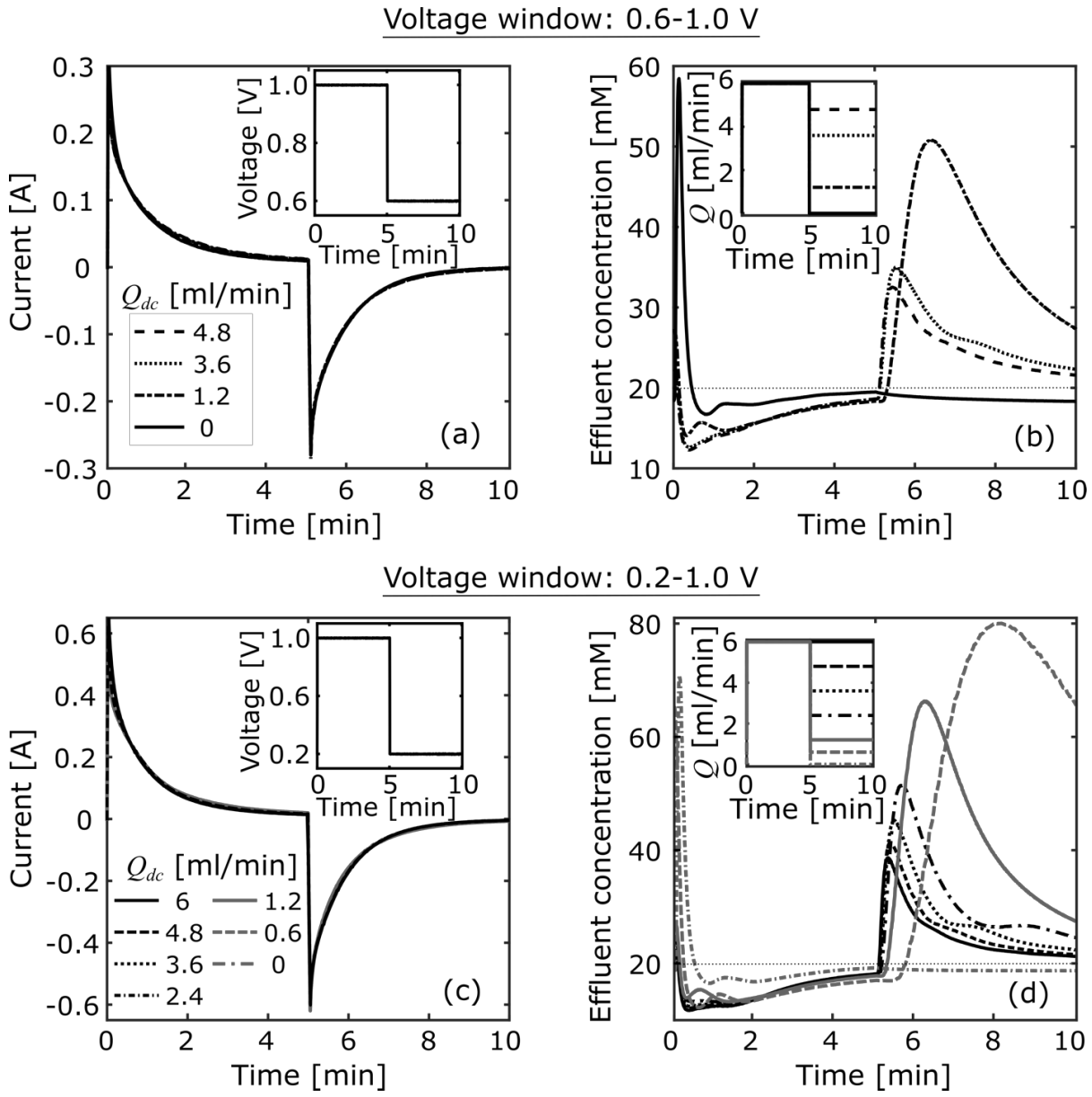

Figure S1: Measured (a) current and (b) effluent concentration as functions of time under dynamic steady state conditions for constant voltage operation between 0.6 and 1.0 V for a flowrate of 6 ml/min during charging, and discharge flowrate values (Q_{dc}) of 0, 1.2, 3.6, and 4.8 ml/min.

Measured time variation of (c) current and (d) effluent concentration under dynamic steady state conditions for constant voltage operation between 0.2 and 1.0 V for a flowrate of 6 ml/min during charging, and discharge flowrate values (Q_{dc}) of 0, 0.6, 1.2, 2.4, 3.6, 4.8 and 6.0 ml/min. Electrical charging and discharging phase durations are each 5 min. The insets in (a) and (c) show the forcing voltage versus time, and the insets in (b) and (d) show the time variation of flowrate. Note that the electrical response is nearly identical for different values of discharge flowrates.

2. Charge transferred and energy consumption for constant voltage and variable flowrate operation

Figure S2a shows measured net electrical charge input and output for each of the two voltage windows. Figure S2b shows the corresponding values of energy consumption and recovery. These results correspond to the experimental results presented in Figures 2 and S1. Note that for a given voltage window, the electrical charge input and output, and energy consumed and recovered, are nearly the same for varying discharge flowrate values. This highlights that the electrical response of CDI is less sensitive to variation in flowrates.

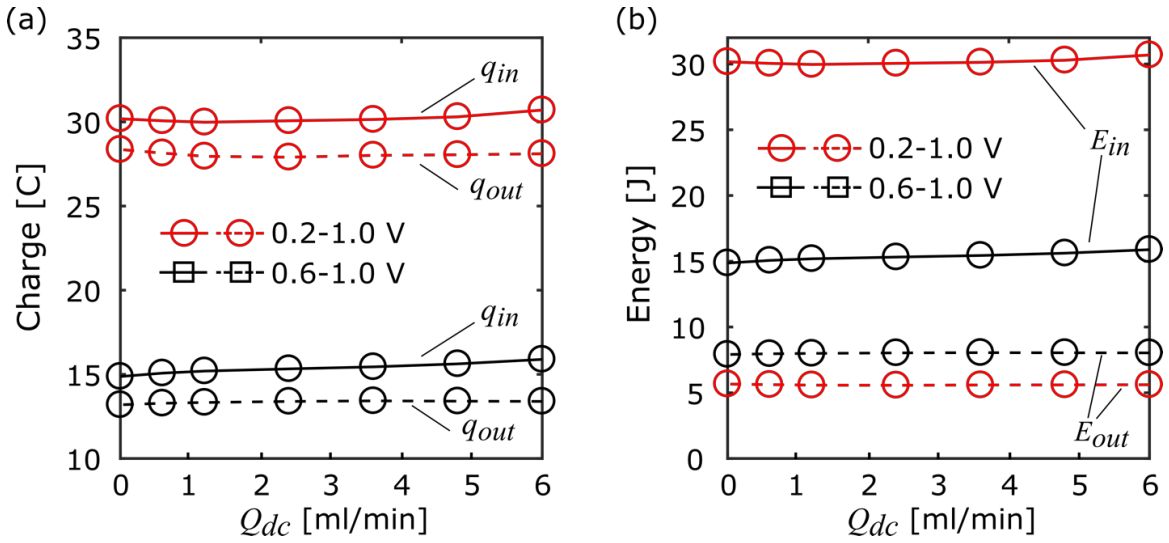

Figure S2: Measured (a) electrical charge input (q_{in}) and output (q_{out}) in Coulombs, and (b) energy consumption (E_{in}) and recovery (E_{out}) in Joules, versus discharge flowrate for the variable flowrate and constant voltage operation between 0.2-1.0 V and 0.6-1.0 V. The flowrate during charging was fixed at 6 ml/min and the flowrate during discharge (Q_{dc}) was varied between 0 to 6 ml/min.

3. Effluent concentration and voltage response versus time for constant current and variable flowrate operation

Figure S3 shows raw experimental measurements for voltage and effluent concentration versus time for two constant current operations subject to the same voltage window of 0.2-1.0 V. The start of the charging or discharge phases are determined by the times at which the measured voltages reached the minimum and maximum voltages of the window, respectively.

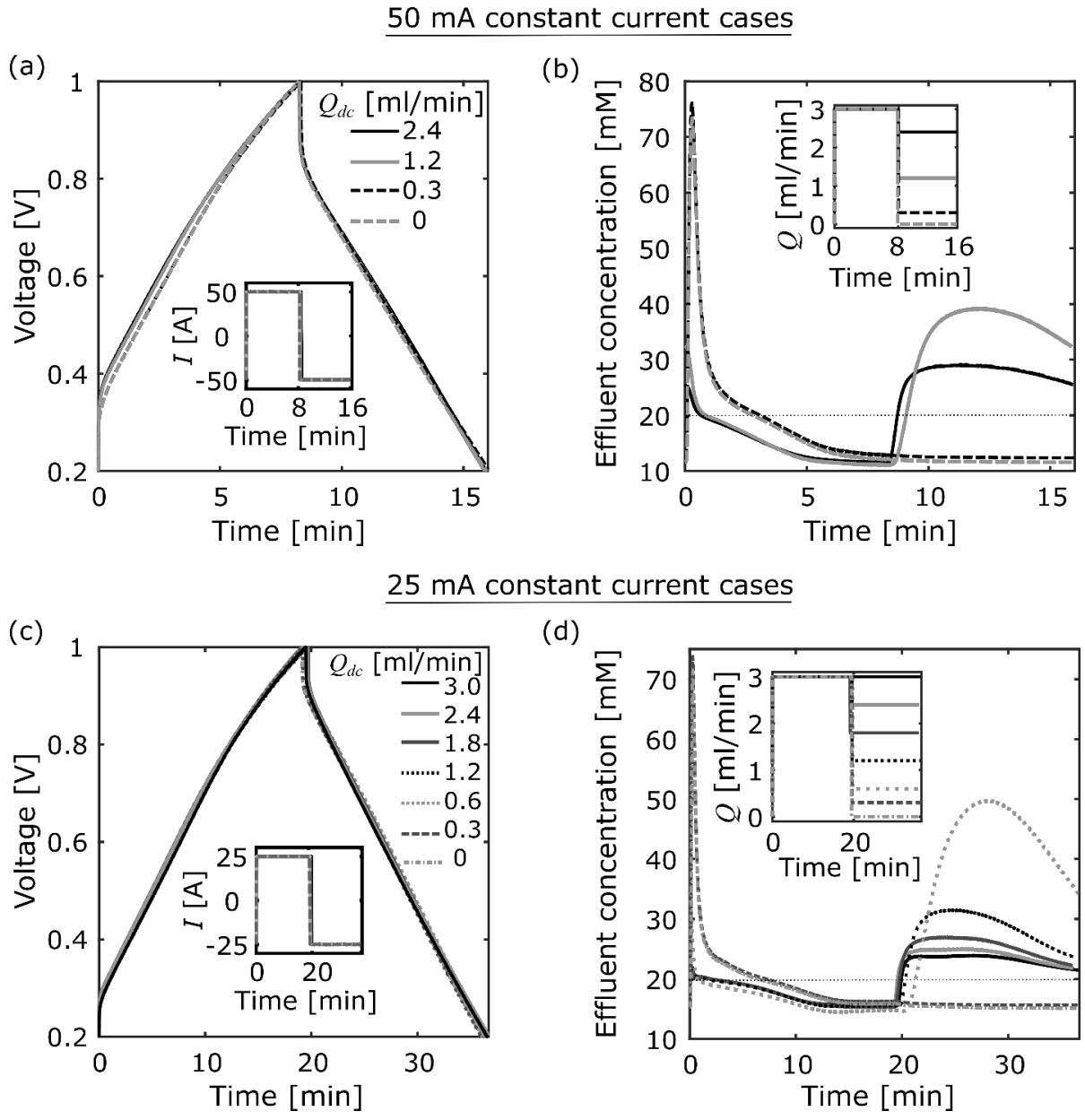

Figure S3: Measured time variation of (a) voltage, and (b) effluent concentration under dynamic steady state conditions for constant current charge-discharge operation at ±50 mA for a flowrate

of 3 ml/min during charging, and for discharge flowrate values (Q_{dc}) of 0, 0.3, 1.2, and 2.4 ml/min. Measured (c) voltage, and (b) effluent concentration versus time under dynamic steady state conditions for constant current charge-discharge operation at ±25 mA for a flowrate of 3 ml/min during charging, and for discharge flowrate values (Q_{dc}) of 0, 0.3, 0.6, 1.2, 1.8, 2.4, and 3.0 ml/min. The insets in (a) and (c) show the time variation of forcing current, and the insets in (c) and (d) show flowrate waveforms versus time.

4. Charge transferred and energy consumption for constant current and variable flowrate operation

Figure S4a shows measured net electrical charge input and output for each of the two applied current values. Figure S2b shows the corresponding values of energy consumption and recovery. These results correspond to the experimental results presented in in Figures 5 and S3. Note that for a given constant current operation, the electrical charge input and output, and energy consumed and recovered, are nearly the same (less than 5% variation) for varying discharge flowrate values.

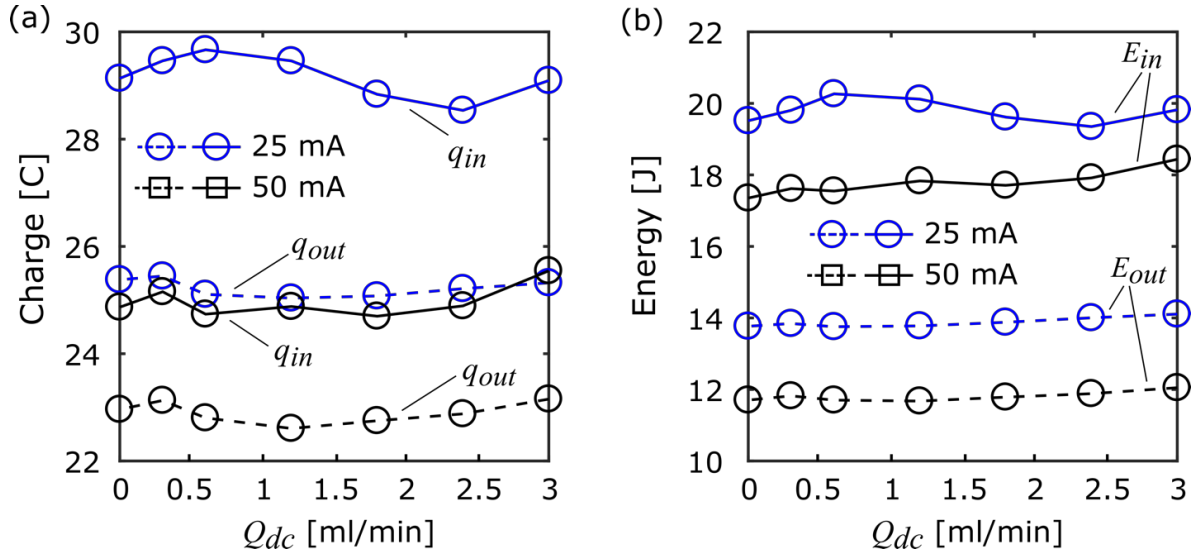

Figure S4: Measured (a) charge input (q_{in}) and output (q_{out}) in Coulombs, and (b) energy consumption (E_{in}) and recovery (E_{out}) in Joules, versus discharge flowrate for the variable flowrate and constant current operation at 25 and 50 mA between 0.2-1.0 V. The flowrate during charging was fixed at 3 ml/min and the flowrate during discharge (Q_{dc}) was varied between 0 to 3 ml/min.

5. Volume of dilute and brine solutions produced per cycle for constant current and variable flowrate operation

Lastly, Figure S5 shows measured volumes of diluent (desalted water output) and output brine per CDI cycle. These data correspond to the experimental results presented in Figures 5 and S3.

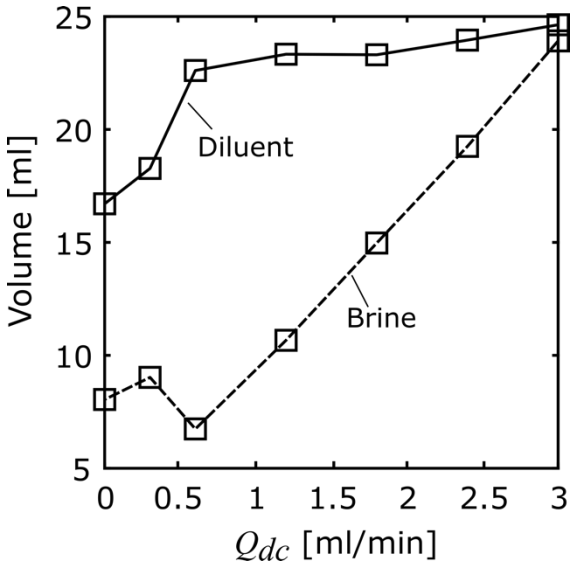

Figure S5: Measured volumes of desalted and brine water generated per cycle versus discharge flowrate for constant current and variable flowrate operation at 50 mA. The flowrate during charging was fixed at 3 ml/min and the flowrate during discharge (Q_{dc}) was varied between 0 to 3 ml/min. See inset of Figure 6a for data corresponding to operation at 25 mA.